Port-Hamiltonian modeling and control of a curling HASEL actuator ⋆

Nelson Cisneros, **Yongxin Wu** , **Kanty Rabenorosoa**, **Yann Le Gorrec**

FEMTO-ST institute, UBFC, CNRS, Besançon, France.(emails: nelson.cisneros@femto-st.fr, yongxin.wu@femto-st.fr, rkanty@femto-st.fr, yann.le.gorrec@femto-st.fr)

Abstract: This paper is concerned with the modeling and control of curling Hydraulically Amplified Self-healing Electrostatic (HASEL) actuators using the port-Hamiltonian approach. For that purpose, we use a modular approach and consider the HASEL actuator as an interconnection of elementary subsystems. Each subsystem is modeled by an electrical component consisting of a capacitor in parallel with an inductor, and a mechanical part based on linear and torsional springs joined to a mass.We identify and validate the model in the experimental setup. Position control is achieved by using Interconnection and Damping Assignment-Passivity Based Control (IDA-PBC) with integral action (IA) for disturbance rejection. Simulation results show the efficiency of the proposed controller.

Keywords: Soft actuator, HASEL actuator, Port-Hamiltonian systems, IDA-PBC design.

1. INTRODUCTION

In recent years one of the most interesting technologies in the soft robotics field is the Hydraulically Amplified Self-healing Electrostatic (HASEL) actuator (Acome et al., 2018).

HASEL actuators blend the advantages of Dielectric Elastomer Actuators (DEAs) and fluid-driven soft actuators, combining the convenience of electrical control, excellent electromechanical performance, extensive design flexibility, and various actuation modes.(Rothemund et al., 2021). There are different types of HASEL actuators, such as peano, planar, elastomeric donut, quadrant donut, high-strain peano, and curling actuators. Some interesting applications of HASEL actuators can be found in the literature: a soft gripper for aerial object manipulation (Kim and Cha, 2021), an actuator powering a robotic arm (Acome et al., 2018), an electro-hydraulic rolling soft wheel (Ly et al., 2022), a peano actuator for enhanced strain, load, and rotary motion (Tian et al., 2022) and soft-actuated joints based on the hydraulic mechanism used in spider legs (Kellaris et al., 2021).

We want to study the bending motion because it is valuable for modeling and controlling more complex actuators for example actuators that can mimic fingers. To get a curling HASEL actuator, a strain limiting layer is added to change the mechanism from linear to angular deformation (Rothemund et al., 2021). It is important to have a reliable model that can represent the system's dynamics to control the actuator. Recent works present frameworks to model HASEL actuators. In (Volchko et al., 2022), Dynamic Mode Decomposition with Control (DMDc) is applied to derive a linear model., approximating the system dynamics. The authors in (Hainsworth et al., 2022) introduce a non-linear reduced-order mass-spring-damper (MSD) model for a HASEL actuator. However, we can not use these frameworks directly because we want to capture the system dynamics and model the mechanical and electrical parts of HASEL actuators.

Port-Hamiltonian (PH) models are well adapted to represent multi-physical systems. PH approach is then an excellent candidate to represent dynamics of the HASEL actuator. Interconnection and Damping Assignment-Passivity Based Control (IDA-PBC) serves as a highly effective tool for generating asymptotically stabilizing controllers for Port-Controlled Hamiltonian (PCH) models. (Ortega et al., 2002). There are previous works using PHS to model soft robots with energy shaping and IDA-PBC controllers showing good results. In (Franco et al., 2021b) and (Franco et al., 2021a), the energy shaping controllers are used to control the position of a soft continuum manipulator with large number of degrees of freedom (DOF). In (Ayala et al., 2022), the IDA-PBC method has been successfully used to a nonlinear Cosserat rod model using an early lumping approach. More recently, the authors in (Yeh et al., 2022) present a port Hamiltonian model with one DOF of a HASEL planar actuator controlling the position using IDA-PBC with Integral Action (IA). Comparing with (Yeh et al., 2022) we model an actuator with bending motion instead of the linear deformation, this introduces nonlinearities in the interconnection matrix. We model the end position drift effect. The main contributions of this paper are:

- We modeled a curling HASEL actuator using the port-Hamiltonian approach, to capture both the electrical and mechanical dynamics of the actuator.
- We identify the model comparing with experimental data and we validated it with different input voltages.

⋆ This work is supported by the EIPHI Graduate School (contract ANR-17-EURE-0002).

- We designed an IDA-PBC controller to control the end point position of the curling HASEL actuator. We add IA to reject disturbances and model uncertainties.

This paper is organized as follows: Section 2 shows the experimental setup. Section 3 presents the model of curling HASEL actuator.We present the parameter's model identification in Section 4. In Section 5 the controller design is presented. Section 6 presents the simulation results and the conclusions are found in Section 7.

2. EXPERIMENTAL SETUP

The experimental setup is shown in Fig. 1. To measure the position, we used a profile laser, Keyence LJ-V7080. We use the high voltage amplifier Trek model 610E. The HASEL actuator is an Artimus Robotics. We use a dSPACE card CLP1104 to send and receive signals from the laser position sensor and the high voltage amplifier.

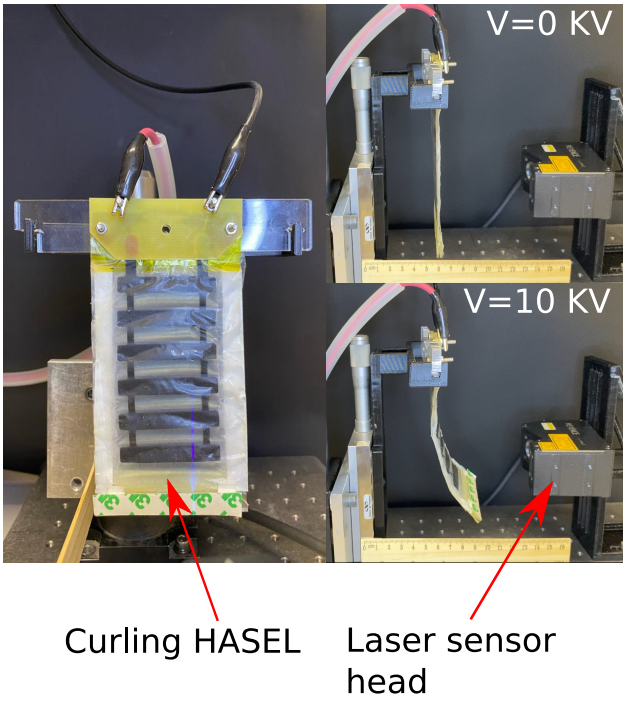

Fig. 1. Experimental setup laser sensor and curling HASEL. The right figures show the actuator deformation. Applying high voltage, the actuator can achieve a horizontal displacement of approximately 3 [cm].

3. MODELING CURLING HASEL ACTUATOR

In this section, we represent the description and the working principle of the curling HASEL actuator. We present the curling HASEL model.

3.1 HASEL actuator description and hypothesis

The curling HASEL actuator is a planar HASEL attached to a strain limiting layer to get the bending actuation. The curling HASEL actuator bends when high voltage is applied.

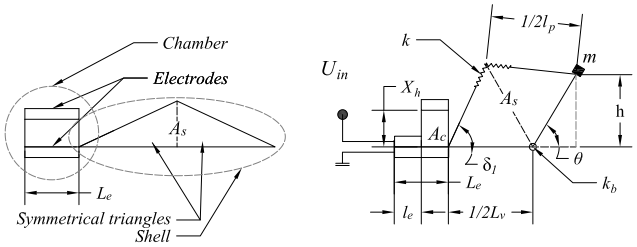

Fig. 2. Basic subsystem. Left: electrodes are totally unzipped. Right: Electrodes are partially zipped when voltage is applied. The shell is deformed.

The curling HASEL actuator consists of a polymer shell filled with dielectric liquid and half covered by a pair of electrodes. When an electric field is applied on the electrodes, it creates Maxwell stress acting the shell which pushes the dielectric liquid inside of the shell. This Hydraulic pressure changes the shape of the shell and drives the movement of the actuator. When the shell is deformed there is a planar displacement, generating forces due the hydraulic amplification principles (Rothemund et al., 2021).

We consider that the actuator depth is uniform, so we do a two dimension analysis. We model an actuator conformed by subsystems. We separate each subsystem model into a chamber and a shell. The chamber is the area between the electrodes whilst the shell will receive the dielectric liquid when the electrodes are zipped. The total volume (volume of the shell plus the volume of the chamber) is considered constant and the dielectric liquid is in-compressible. The bending of the bottom film is modeled as a torsional spring. The top film of the shell is considered to be elongable and contains mechanical energy. The elongation is modeled as a linear spring. The volume of the dielectric liquid in the chamber is transferred to the shell depending of the applied voltage. The electrical part of the actuator is conformed by the electrodes. The electrodes are modeled with a variable capacitor. The model considers a variable length of the zipped electrodes. The zipped electrodes length depends on the applied voltage. The distance between the unzipped electrodes part is considered constant, see Fig. 2.

3.2 Geometric relations

In this part, we present the geometric relations that link the angle θ with the zipped electrodes length l_e. Then, from θ we can derive the actuator position $h(\theta)$, i.e., the displacement of the actuator end position.

It is crucial to obtain a relation between θ and l_e because the electrode's capacitance can be presented as a function of l_e. Therefore it allows us to relate the electrical charge that depends on the capacitance with the derivative of the electrical energy respecting the angle θ, joining the electrical and the mechanical part.

We represent the chamber as a rectangular area and the shell is modeled as two symmetric triangles. Fig. 2 shows the model variables of a basic subsystem. Next equations allow to find the relation between the θ angle and the zipped electrodes length l_e.

The area inside the shell is:

$$A_s = \frac{1}{4} l_p L_v sin(\delta_1) \tag{1}$$

with

$$\delta_1 = \frac{\pi + \theta}{2} - \sin^{-1}\left(\frac{L_v}{l_p}\sin\left(\frac{\pi - \theta}{2}\right)\right). \tag{2}$$

The total area is:

$$A_T = A_s + X_h(L_e - l_e), \tag{3}$$

where, L_v and l_p are the bottom and the top film. X_h is the height of the chamber and L_e is the length of the chamber.

The zipped electrodes length is:

$$l_e = L_e - \frac{1}{X_h}\left(A_T + \frac{L_v l_p}{4} sin(\delta_1)\right). \tag{4}$$

3.3 Curling HASEL port-Hamiltonian model

In this section we present the port-Hamiltonian model for the curling HASEL actuator. First, we briefly recall the port-Hamiltonian model from (van der Schaft, 2000):

$$\begin{aligned} \dot{x} &= [J(x) - R(x)]\frac{\partial H}{\partial x}(x) + g(x)u; \\ y &= g^T(x)\frac{\partial H}{\partial x}(x), \end{aligned} \tag{5}$$

where $J(x) = -J^T(x)$ is the interconnection matrix, $R(x) = R^T(x) \geq 0$ is the dissipation matrix and H is the total energy of the system (Hamiltonian).

Combining basic subsystems we can represent the overall dynamical behavior of the HASEL actuator. The model can be extended to $n \in \mathbb{N}$ subsystems. The subsystems share the same input voltage.

Fig. 3 shows the schematic of the interconnection of four subsystems. The total energy of the system is composed

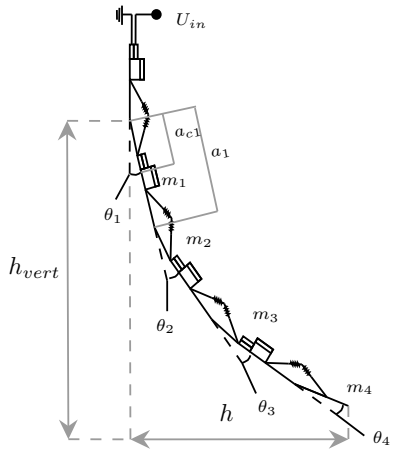

Fig. 3. Four interconnected subsystems. The same voltage is applied to the entire system.

of the next elements:

$$\begin{aligned} H(\theta, l_p, p, \phi, Q) = {} & H_\theta(\theta) + H_{l_p}(l_p) + H_g(\theta) + \\ & H_p(p) + H_\phi(\phi, Q) + H_Q(Q, \phi, \theta, l_p). \end{aligned} \tag{6}$$

The first term of the energy (6) is the potential energy related to the torsional spring:

$$H_\theta = \frac{1}{2}\sum_{i=1}^{n} K_{b_i}\theta_i^2 = \frac{1}{2}\theta^T K_b \theta \tag{7}$$

where $K_b = \text{diag}[K_{b_1}\ K_{b_2}\ \dots\ K_{b_n}]$ is the stiffness matrix and $\theta = [\theta_1\ \theta_2\ \dots\ \theta_n]$ presents the angular vector of each subsystem.

The second term of the energy (6) is the potential energy related to the linear springs:

$$H_{l_p} = \frac{1}{2}\sum_{i=1}^{n} K_i(l_{p_i} - L_{p_i})^2 = \frac{1}{2}(l_p - L_p)^T K (l_p - L_p), \tag{8}$$

where $K = \text{diag}[K_1\ K_2\ \dots\ K_n]$ and $l_p^T = [l_{p_1}\ l_{p_2}\ \dots\ l_{p_n}]$. The total potential energy related to the gravity is:

$$H_{\text{g}} = \sum_{i=1}^{n} H_{g_i} \tag{9}$$

The kinetic energy is then given by:

$$H_p = \frac{1}{2} p^T M^{-1} p, \tag{10}$$

where M is the matrix of inertia and p is the vector of angular momentum $p^T = [p_1\ p_2\ \dots\ p_n]$.

The electrical energy has two components, the energy related to the magnetic flux that allows us to represent the drift effect and the energy related with the charge. The inductor discharges the capacitor along the time.

$$H_\phi = \frac{1}{2}\sum_{i=1}^{n} \frac{\phi_i^2}{L_i} = \frac{1}{2}\phi^T L^{-1}\phi \tag{11}$$

The energy stored in the capacitor is:

$$H_Q = \frac{1}{2}\sum_{i=1}^{n} \frac{Q_i^2}{C_{s_i}} = \frac{1}{2} Q^T C^{-1} Q, \tag{12}$$

where $\phi^T = [\phi_1\ \phi_2\ \dots\ \phi_n]$ is the magnetic flux, L is the inductance of the equivalent electric circuit $L = \text{diag}[L_1\ L_2\ \dots\ L_n]$. $C = \text{diag}[C_{s_1}\ C_{s_2}\ \dots\ C_{s_n}]$ is the capacitance of the equivalent electric circuit and $Q = [Q_1\ Q_2\ \dots\ Q_n]^T$ is the charge. The capacitance of the zipped part of the electrodes is $C_{1_i} = \frac{\epsilon_0 \epsilon_r w l_{e_i}}{2t}$, the capacitance of the unzipped part is $C_{2_i} = \frac{\epsilon_0 \epsilon_r w (L_e - l_{e_i})}{2t + X_h}$ the capacitance of one subsystem is $C_{s_i} = C_{1_i} + C_{2_i}$. The input gain is $ga^T = [ga_1\ ga_2\ ...\ ga_n]$. To capture the nonlinearities of the system the input gain is a nonlinaer function that depends of the angular position $ga_i = \gamma_1 \cos(\gamma_2 \theta_i)$. The inverse value of the equivalent electric circuit resistance is defined as the matrix $\bar{R} = \text{diag}[\frac{1}{R_1}\ \frac{1}{R_2}\ ...\ \frac{1}{R_n}]$. The damping system is $b = \text{diag}[b_1\ b_2\ ...\ b_n]$. The resistance associated to the inductance is $r_L = \text{diag}[r_{L_1}\ r_{L_2}\ ...\ r_{L_n}]$. We define the term $d = \text{diag}\left(\frac{2A_s}{l_p}\right)$. The proposed port-Hamiltonian model of the curling HASEL actuator is:

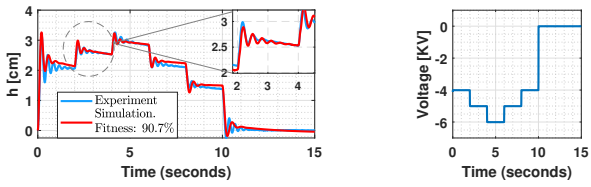

(a) (b)

Fig. 4. (4a) Model identification, fitness: 90.7%. (4b) Input signal.

$$\underbrace{\begin{bmatrix}\dot{\theta}\\ \dot{l_p}\\ \dot{p}\\ \dot{\phi}\\ \dot{Q}\end{bmatrix}}_{\dot{x}} = \underbrace{\begin{bmatrix}0 & 0 & I & 0 & 0\\ 0 & 0 & d & 0 & 0\\ -I & -d & -b & 0 & 0\\ 0 & 0 & 0 & -r_L & I\\ 0 & 0 & 0 & -I & -\bar{R}\end{bmatrix}}_{J-R} \underbrace{\begin{bmatrix}\nabla_\theta H\\ \nabla_{l_p} H\\ \nabla_p H\\ \nabla_\phi H\\ \nabla_Q H\end{bmatrix}}_{\nabla_x H} + \underbrace{\begin{bmatrix}0\\ 0\\ 0\\ 0\\ \bar{R}ga(\theta)\end{bmatrix}}_{g} U_{in}; \quad (13)$$

$$y = \underbrace{(\bar{R}ga(\theta))^T C^{-1} Q}_{g^T \nabla_x H}.$$

The output $y = i_e$ is the current that is the power conjugated variable of the input voltage. The energy balance equation can be computed as:

$$\begin{aligned}\frac{\partial H}{\partial t} &= -\frac{\partial H^T}{\partial x} R \frac{\partial H}{\partial x} + y^T u;\\ \frac{\partial H}{\partial t} &\leq y^T u = i_e U_{in}.\end{aligned} \quad (14)$$

4. MODEL IDENTIFICATION AND VALIDATION

We identified the sensitive parameters through simulation. We use the Levenberg–Marquardt optimization algorithm (MathWorks, 2020) to obtain the parameters K_b, b, L, γ_1 and γ_2. We show the system identification results that consists of four interconnected subsystems in Fig. 4. We validated the model with two datasets, one with negative inputs and another with positive inputs, as shown in Fig. 5.

The fitness between the model and the experimental data was computed with the fit values that represents the error norm with the normalized root mean squared error (NRMSE) as the cost function.

$$fit(i) = \frac{\| x_{ref}(:) - x_{data}(:) \|}{\| x_{ref}(:) - (x_{ref}(:)) \|} \quad (15)$$

where $\| \cdot \|$ is the 2-norm of a vector.

Then we use a the Matlab command *goodnessOfFit* with the cost function NRMSE to obtain the model fitness. The identified parameters are shown in Table 1.

5. POSITION CONTROL DESIGN

In this work, we want to control the end point position of the curling HASEL actuator. To this end, we propose an IDA-PBC design method. This method aims to find a state feedback control law $\beta(x)$ so that we can map the open-loop system to a closed-loop system with the desired behavior in the following form.

$$\dot{x} = (J_d - R_d)\nabla_x H_d. \quad (16)$$

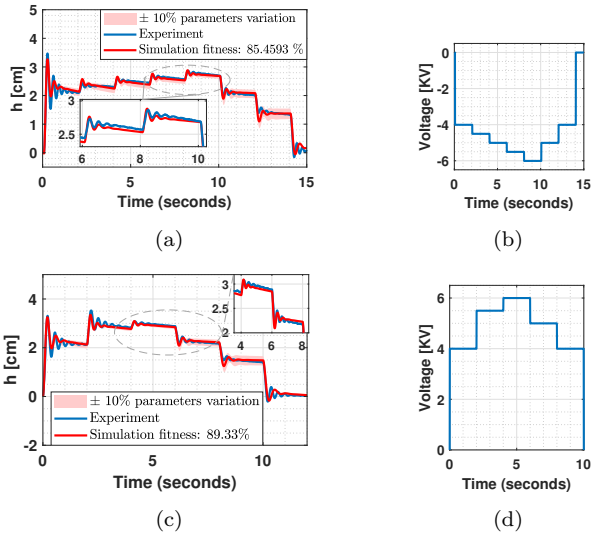

(a) (b) (c) (d)

Fig. 5. (5a) Model validation, negative input fitness: 85.46% (5b) Input signal. 5c) Model validation, positive input fitness: 89.33% (5d) Positive input signal. We can observe the model's behavior in response to a variation of 10% around the nominal values.

Symbol	Value	Units	Definition
L_p	0.015	m	Length of top film
L_v	0.015	m	Length of bottom film
L_e	0.015	m	Length of electrodes
X_h	0.002	m	Chamber high
m	0.047	kg	Mass
ϵ_r	2.2	F/m	Relative permittivity
ϵ_0	$8.854\text{x}10^{-12}$	F/m	Vacuum permittivity
w	0.05	m	Actuator width
t	$18\text{x}10^{-}6$	m	Film thickness
R_i	10	Ω	Resistance
r_L	20	Ω	Resistance
L	150	F	Inductance
K	200	N/m	Spring constant
K_b	0.202	Nm/rad	Torsional spring constant
b	0.0199	kgs	Damping
γ_1	104.33	-	Gain parameter
γ_2	7.67	-	Gain parameter

Table 1. Model parameters.

Fig. 6 shows the control scheme. The desired equilibrium points x^* (θ^*, l_p^* ϕ^* and Q^*) and the state variables x (θ, l_p, ϕ and Q) are the controller ($\beta(x)$) inputs. We can define the desired interconnection and dissipation matrix as:

$$J_d - R_d = \begin{bmatrix}0 & 0 & J_{13} & 0 & \alpha_1\\ 0 & 0 & J_{23} & 0 & \alpha_2\\ -J_{13} & -J_{23} & -r_{33} & J_{43} & \alpha_3\\ 0 & 0 & -J_{43} & 0 & \alpha_4\\ -\alpha_1 & -\alpha_2 & -\alpha_3 & -\alpha_4 & -r_{55}\end{bmatrix}, \quad (17)$$

where J_{13}, J_{23}, J_{43}, α_1, α_2, α_3 and α_4 are the control design parameters to be determined. The desired total energy can be defined with the desired equilibrium position of the actuator as:

$$\begin{aligned}H_d = &(\theta - \theta^*)^T \tilde{K_b}(\theta - \theta^*) + (l_p - l_p^*)^T \tilde{K}(l_p - l_p^*)\\ &+P^T M^{-1} P + (\phi - \phi^*)^T \tilde{K_\phi}(\phi - \phi^*)\\ &+(Q - Q^*)^T \tilde{K_Q}(Q - Q^*)\end{aligned} \quad (18)$$

The derivative of the desired total energy respected to the state variables is

$$\nabla_x H_d = \begin{bmatrix} \tilde{K_b}(\theta - \theta^*) \\ \tilde{K}(l_p - l_p^*) \\ M^{-1}p \\ \tilde{K_\phi}(\phi - \phi^*) \\ \tilde{K_Q}(Q - Q^*) \end{bmatrix}. \tag{19}$$

To get a state feedback matching the closed-loop system with a desired PH system $\dot{x} = (J_d - R_d)\nabla_x H_d$ defined above. We need to solve the following matching conditions

$$g^\perp [J - R]\nabla_x H = g^\perp [J_d - R_d]\nabla_x H_d, \tag{20}$$

with $g^\perp$ is a full rank annihilator of the input matrix g. One can choose the annihilator as following:

$$g^\perp = \begin{bmatrix} 1 & 0 & 0 & 0 & 0 \\ 0 & 1 & 0 & 0 & 0 \\ 0 & 0 & 1 & 0 & 0 \\ 0 & 0 & 0 & 1 & 0 \end{bmatrix}. \tag{21}$$

We find J_{13}, J_{23}, J_{43} as a function of α_1, α_2, α_3 and α_4.

$$J_{13} = \text{diag}((\text{diag}(M^{-1}p))^{-1}(M^{-1}p - \alpha_1 \tilde{K_Q}(Q - Q^*))); \tag{22}$$

$$J_{23} = \text{diag}((\text{diag}(M^{-1}p))^{-1}(dM^{-1}p - \alpha_2 \tilde{K_Q}(Q - Q^*))); \tag{23}$$

$$\begin{aligned} r_{33} =& \text{diag}((\text{diag}(M^{-1}p))^{-1}(\nabla_\theta H + d\nabla_{l_p} H + bM^{-1}p \\ &+ \alpha_3 \tilde{K_Q}(Q - Q^*) - J_{13}\tilde{K_b}(\theta - \theta^*) - J_{23}\tilde{K}(l_p - l_p^*) \\ &+ J_{43}\tilde{K_\phi}(\phi - \phi^*))). \end{aligned} \tag{24}$$

$$J_{43} = \text{diag}((\text{diag}(M^{-1}p))^{-1}(r_L L^{-1}\phi - C^{-1}Q + \alpha_4 \tilde{K_Q}(Q - Q^*)); \tag{25}$$

We obtain the control law considering the next design parameters $\alpha_1 = I$, $\alpha_2 = 0$, $\alpha_3 = I$ and $\alpha_4 = 0$.

$$\begin{aligned} \beta(x) = & (\bar{R}ga^T \bar{R}ga)^{-1}\bar{R}ga^T(-\tilde{K_b}(\theta - \theta^*) - M^{-1}p \\ & -r_{55}\tilde{K_Q}(Q - Q^*) + L^{-1}\phi + (\bar{R}C^{-1}Q)), \end{aligned} \tag{26}$$

Fixing l_p^* and θ^* we can find Q^* from the model in steady state. To ensure the stability of the closed loop system, the desired damping r_{33} should be greater than or equal to zero $r_{33} \geq 0$, thus the desired charge must be smaller or equal to:

$$\begin{aligned} Q^* \leq & \; Q - (\text{diag}(\nabla_\theta H_d + I)^{-1}\text{diag}(\bar{K_Q})^{-1}(\nabla_\theta H_d - \\ & \nabla_\theta H - d\nabla_{l_p} H - b\nabla_p H - J_{23}\nabla_{l_p} H_d - J_{43}\nabla_\phi H_d) \end{aligned} \tag{27}$$

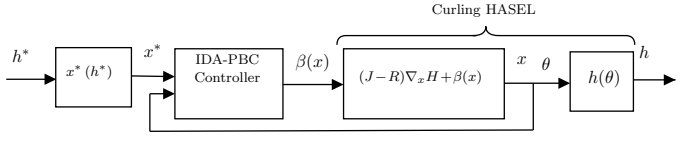

Fig. 6. Closed-loop scheme with the controller $\beta(x)$ inputs are the state variables x and the desired values x^*. The system input is the necessary voltage computed by the controller. $h(x)$ is the function that allows to find the final position as a function of each link angle.

5.1 Disturbance rejection using Integral Action

In this subsection, we want to improve the robustness of the controller (26) with the unknown mass load on the actuator using a structure-preserving integral action. The unknown mass load can be regarded as the unactuated external force disturbance (d_u), also the integral action controller can reject actuated disturbances (d_a). The disturbed closed loop system with (26) can be written as:

$$\begin{bmatrix} \dot{Q} \\ \dot{\theta} \\ \dot{l_p} \\ \dot{p} \\ \dot{\phi} \end{bmatrix} = [J_d - R_d] \begin{bmatrix} \nabla_Q H_d \\ \nabla_\theta H_d \\ \nabla_{l_p} H_d \\ \nabla_p H_d \\ \nabla_\phi H_d \end{bmatrix} + \begin{bmatrix} d_a \\ 0 \\ 0 \\ d_u \\ 0 \end{bmatrix}, \tag{28}$$

where the desired interconnection and the damping matrix are defined as:

$$J_d(x) := \left[\begin{array}{c|c} J_{aa}(x) & J_{au}(x) \\ \hline -J_{au}^T(x) & J_{uu}(x) \end{array}\right] = \left[\begin{array}{c|cccc} 0 & -\alpha_1 & -\alpha_2 & -\alpha_3 & -\alpha_4 \\ \hline \alpha_1 & 0 & 0 & -J_{13} & 0 \\ \alpha_2 & 0 & 0 & -J_{23} & 0 \\ \alpha_3 & J_{13} & J_{23} & 0 & -J_{43} \\ \alpha_4 & J_{13} & 0 & J_{43} & 0 \end{array}\right]; \tag{29}$$

$$R_d(x) := \left[\begin{array}{c|c} R_{aa}(x) & R_{au}(x) \\ \hline R_{au}^T(x) & R_{uu}(x) \end{array}\right] = \left[\begin{array}{c|cccc} r_{55} & 0 & 0 & 0 & 0 \\ \hline 0 & 0 & 0 & 0 & 0 \\ 0 & 0 & 0 & 0 & 0 \\ 0 & 0 & 0 & r_{33} & 0 \\ 0 & 0 & 0 & 0 & 0 \end{array}\right]. \tag{30}$$

Using the method described in (Ferguson et al., 2017). We can choose the new closed loop Hamiltonian as:

$$H_{cl} = H_d + \frac{K_i}{2}\|Q - x_c\|^2 \tag{31}$$

and the new closed loop system can be derived as:

$$\left[\begin{array}{c} \dot{x}_a \\ \hline \dot{x}_u \\ \hline \dot{x}_c \end{array}\right] = (J_{cl} - R_{cl}) \left[\begin{array}{c} \nabla_{x_a} H_{cl} \\ \hline \nabla_{x_u} H_{cl} \\ \hline \nabla_{x_c} H_{cl} \end{array}\right] + \left[\begin{array}{c} d_a \\ \hline 0 \\ 0 \\ d_u \\ 0 \\ \hline 0 \end{array}\right]. \tag{32}$$

One can thus get a structure preserving Integral action (IA) controller:

$$\begin{aligned} u_i = & \; [-J_{aa} + R_{aa} + J_{c_1}(x) - R_{c_1}(x) - R_{c_2}(x)]\nabla_{x_a} H + \\ & [J_{c_1}(x) - R_{c_1}(x)]K_i(x_a - x_c) + 2R_{au}\nabla_{x_u} H; \\ \dot{x_c} = & -R_{c_2}(x)\nabla_{x_a} H + (J_{au} + R_{au})\nabla_{x_u} H, \end{aligned} \tag{33}$$

where u_i is the output of the IA controller. x_c is the IA controller state. The actuated state is the charge Q_m whilst the unactuated states are the angle θ, the length l_p, the angular momentum p and the magnetic flux ϕ.

Being $J_{au} = -[\alpha_1 \; 0 \; \alpha_3 \; 0]$ and $J_{c_1} = R_{c_2} = R_{au} = 0$ and $R_{c_1} = r_{55}$ we obtain the next control law.

$$\begin{aligned} u_i = & \; -r_{55}K_i(Q - x_c); \\ \dot{x_c} = & -(\alpha_1 \tilde{K_b}(\theta - \theta^*) + \alpha_3 M^{-1}p). \end{aligned} \tag{34}$$

Where the K_i parameter design is chosen as a vector of dimensions $1 \times n$. The $\beta(x)$ controller dimension is 1×1. The control scheme is shown in Fig. 7 and the

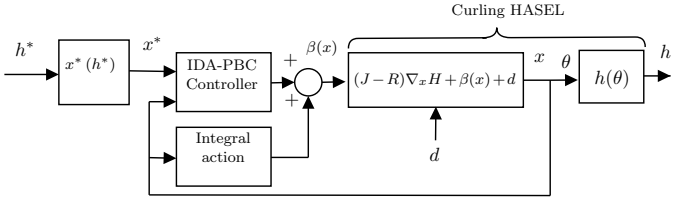

Fig. 7. Closed-loop scheme with IA.

interconnection and damping matrix are given as:

$$J_{cl} \coloneqq \begin{bmatrix} 0 & J_{au} & 0 \\ -J_{au}^T & J_{uu} & 0 \\ 0 & 0 & 0 \end{bmatrix}; \quad R_{cl} \coloneqq \begin{bmatrix} r_{55} & 0 & r_{55} \\ 0 & r_{33} & 0 \\ r_{55} & 0 & r_{55} \end{bmatrix}. \tag{35}$$

6. NUMERICAL SIMULATION

In this section, we show the numerical simulation results using the proposed control method. The open loop parameters are given in Table. 1. We implement the IDA-PBC controller (26) with the Integral action controller (34) to achieve the desired end point position of the curling actuator. To show the different closed loop dynamics behaviour, we vary the tuning parameter $\tilde{K}_b$ while keep the rest of the tuning parameters constant. The controller parameters values are $r_{55} = \text{diag}([0.1\ 0.1\ 0.1\ 0.1])$ and $K_i = [0\ 150\ 0\ 0]$. One can observe the end point regulation to the desired position in Fig. 8 and the external disturbance rejection Fig. 9.

Fig. 8 presents actuator displacement when we vary the tuning value $\tilde{K}_b$, maintaining fixed the $\tilde{K}_Q$ value. The desired position of the end point is $h^*(\theta) = 2$ cm. From the simulation results in Fig. 8, one can observe that the response time of the closed-loop system becomes faster as the value of $\tilde{K}_b$ increases, because $\tilde{K}_b$ is the closed loop stiffness.

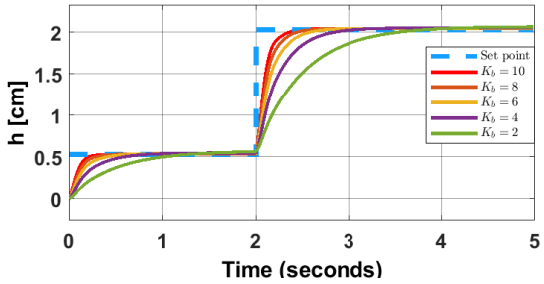

Fig. 8. Position control keeping constant the parameters $\tilde{K}_Q = 1000$, the set-point equal to $2[cm]$ and varying the tuning parameter related with the desired angle $\tilde{K}_b$.

Fig. 9 shows the actuator displacement to the desired set point. The external unactuated disturbance disturbance is added at $3[s]$ and the actuated disturbance is added at $7[s]$. The proposed controller with integral action can compensate the disturbances.

7. CONCLUSION

We model and control a curling HASEL actuator in this work using the port-Hamiltonian approach. The dynamics of the actuator is divided into two parts. One part is the mechanical part described by linear and torsional springs, and the deformable capacitor and the inductor represent the other part of the electronic system. An IDA-PBC controller has been proposed with the integral action to control the position of the actuator. It was shown that the controller follows the set point, and we can adjust the dynamics performance by varying the controller tuning parameter. The robustness of the controller regarding the external disturbance has been improved using the integral action controller.

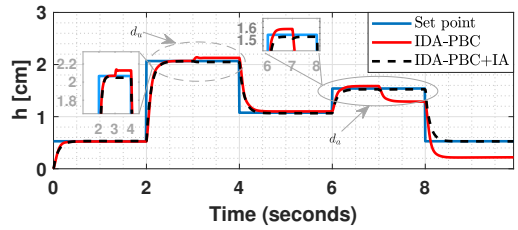

(a)

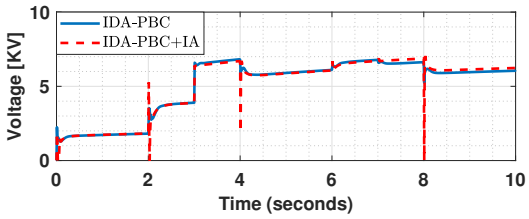

(b)

Fig. 9. (9a) Position control $\tilde{K}_Q = 10$, $\tilde{K}_b = 10$ and $K_i = [0\ 150\ 0\ 0]$. The simulation presents a disturbances d_u and d_a at $3s$ and $7s$ respectively. (9b) IDA-PBC and IDA-PBC+IA control signals.

The perspectives of this work are to implement the proposed IDA-PBC controller with IA, testing the system in closed loop. Furthermore, it could be interesting to model and control more complex structures based on HASEL actuators (e.g., scorpion, fish, human hands-inspired designs) with the interconnection of basic subsystems.

REFERENCES

Acome, E., Mitchell, S.K., Morrissey, T.G., Emmett, M.B., Benjamin, C., King, M., Radakovitz, M., and Keplinger, C. (2018). Hydraulically amplified self-healing electrostatic actuators with muscle-like performance. *Science*, 359(6371), 61–65.

Ayala, E.P., Wu, Y., Rabenorosoa, K., and Le Gorrec, Y. (2022). Energy-based modeling and control of a piezotube actuated optical fiber. *IEEE/ASME Transactions on Mechatronics*, 1–11.

Ferguson, J., Donaire, A., Ortega, R., and Middleton, R.H. (2017). New results on disturbance rejection for energy-shaping controlled port-Hamiltonian systems.

Franco, E., Casanovas, A.G., Tang, J., y Baena, F.R., and Astolfi, A. (2021a). Position regulation in cartesian space of a class of inextensible soft continuum manipulators with pneumatic actuation. *Mechatronics*, 76, 102573.

Franco, E., Garriga-Casanovas, A., Tang, J., y Baena, F.R., and Astolfi, A. (2021b). Adaptive energy shaping control of a class of nonlinear soft continuum manipulators. *IEEE/ASME Transactions on Mechatronics*, 27(1), 280–291.

Hainsworth, T., Schmidt, I., Sundaram, V., Whiting, G.L., Keplinger, C., and MacCurdy, R. (2022). Simulating electrohydraulic soft actuator assemblies via reduced order modeling. In *2022 IEEE 5th International Conference on Soft Robotics (RoboSoft)*, 21–28. IEEE.

Kellaris, N., Rothemund, P., Zeng, Y., Mitchell, S.K., Smith, G.M., Jayaram, K., and Keplinger, C. (2021). Spider-inspired electrohydraulic actuators for fast, soft-actuated joints. *Advanced Science*, 8(14), 2100916.

Kim, S. and Cha, Y. (2021). Double-layered electrohydraulic actuator for bi-directional bending motion of soft gripper. In *2021 18th International Conference on Ubiquitous Robots (UR)*, 645–649.

Ly, K., Mayekar, J.V., Aguasvivas, S., Keplinger, C., Rentschler, M.E., and Correll, N. (2022). Electro-hydraulic rolling soft wheel: Design, hybrid dynamic modeling, and model predictive control. *IEEE Transactions on Robotics*.

MathWorks (2020). Matlab system identification toolbox. natick, massachusetts, united states: The mathworks, inc.

Ortega, R., van Der Schaft, A., Maschke, B., and Escobar, G. (2002). Interconnection and damping assignment passivity-based control of port-controlled Hamiltonian systems. *Automatica*, 38(4), 585–596.

Rothemund, P., Kellaris, N., Mitchell, S.K., Acome, E., and Keplinger, C. (2021). HASEL artificial muscles for a new generation of lifelike robots—recent progress and future opportunities. *Advanced Materials*, 33(19), 2003375.

Tian, Y., Liu, J., Wu, W., Liang, X., Pan, M., Bowen, C., Jiang, Y., Sun, J., McNally, T., Wu, D., et al. (2022). Peano-hydraulically amplified self-healing electrostatic actuators based on a novel bilayer polymer shell for enhanced strain, load, and rotary motion. *Advanced Intelligent Systems*, 2100239.

van der Schaft, A. (2000). *L2-gain and passivity techniques in nonlinear control*. Springer.

Volchko, A., Mitchell, S.K., Morrissey, T.G., and Humbert, J.S. (2022). Model-based data-driven system identification and controller synthesis framework for precise control of siso and miso HASEL-powered robotic systems. In *2022 IEEE 5th International Conference on Soft Robotics (RoboSoft)*, 209–216. IEEE.

Yeh, Y., Cisneros, N., Wu, Y., Rabenorosoa, K., and Gorrec, Y.L. (2022). Modeling and position control of the HASEL actuator via port-Hamiltonian approach. *IEEE Robotics and Automation Letters*, 7(3), 7100–7107.